Chapter 12

Nanostructured Biosensors: Influence of Adhesion Layer, Roughness and Size on the LSPR: A Parametric Study

Sameh Kessentini and Dominique Barchiesi

Additional information is available at the end of the chapter

http://dx.doi.org/10.5772/52906

1. Introduction

The development of nanobiosensors dedicated to early disease diagnosis has an utmost societal interest. The biosensors based on gold nanostructures are known to be efficient and tunable [30, 43]. As an illustration, the objective of the European project *Nanonatenna* (F5-2009 241818) under the "Health" research area of the seventh framework program, is the development of a high sensitive and specific nanosensor based on extraordinary optical signal enhancement dedicated to the in vitro proteins detection and disease diagnosis (cancer, cardiovascular or infectious diseases). The diagnosis process is based on the in vitro detection of the presence of small quantities of the target protein. The consortium of 12 partners works on the design of nanoantennas to reach biosensor high sensitivity. For this, gratings of gold nanoparticles are used to enhance locally the optical signal when excited by an adequate illumination.

The underlying physical phenomenon is the localized surface plasmon resonance (LSPR). The surface plasmon resonance is defined by Raether: "The electron charges on a metal boundary can perform coherent fluctuations which are called surface plasma oscillations" [39]. According to [32], "Localized surface plasmons are non-propagating excitations of the conduction electrons of metallic nanostructures coupled to the electromagnetic field… The curved surface of the particles exerts an effective restoring force of the driven electrons, so that a resonance can arise, leading to field amplification both inside and in the near-field zone outside the particle." The position of the LSPR can therefore be tuned by modifying the shape and size of the nanoparticles. It can be adapted to the specific excitation of molecules deposited on the nanoparticle surface, and the detection of a very few quantity is therefore expected.

A periodic arrangement of nanoparticles is used to increase the sensitivity of the biosensor. The prolate and oblate exhibit LSPRs which are related to their asymmetry, leading to a distribution of energy in different LSPR modes [21]. Coupling between transverse and longitudinal LSPR occurs. To prevent this effect which could decrease the efficiency of the biosensor, gratings of gold cylindric nanoparticles have been extensively studied [11, 19, 21–23, 45]. In that papers, the tuning of the LSPR has been proved by varying the diameter of nanocylinders or seldom their height.

Even if the fabrication process of nanodevices has been continuously improved and more control and precision were achieved [25, 46], the process of deposition of metal on the substrate is subject to incertitudes on the size of the nanostructures that are generally rough. Moreover, a thin intermediate layer (chromium, titanium…) is used to stick gold on substrate. This adhesion layer is usually neglected in simulations, excepted in a few studies for Surface Plasmon Resonance based biosensor [3, 6, 7], and in the case of cylinder-based transducer [42]. Nevertheless in the theoretical and numerical studies, the roughness of the gold nanostructures are neglected and the nanometric adhesion layer of gold on substrate is rarely included.

This chapter is dedicated to the parametric study of a specific nanobiosensor, made of a grating of gold nanocylinders deposited on a dielectric substrate and the goal is to investigate the influence of adhesion layer and roughness on the position of the LSPR as a function of the geometrical parameters of cylinders: their diameter D and height h. The first section is devoted to the validation of the model by comparison to previous simulations with Finite Difference Time Domain [42], and to experimental results [20, 21, 23]. The analysis of the parametric study is given in section 3 and a method to deduce heuristic laws for the LSPR is also proposed, before concluding.

2. The model

2.1. The biosensor

Figure 1 shows a schematic of the biosensor. All the parameters related to the experiments can be found in [23]. A grating of gold nanocylinders is deposited on CaF_2 substrate. The distance between cylinders P is supposed to be fixed to 200 nm. Let us note that the periodicity of the grating may influence the detected position of the LSPR [19, 28], in particular in the case of an homogeneous-evanescent switch of a diffracted order [1, 12]. Experimental studies have shown that a variation of the period $P + D = 200 \pm 50$ nm, leads to a LPSR shift lower than 20 nm [20, p. 67], with $D = 50$ nm and a spectral investigation from 575 nm to 680 nm. [19] observed a redshift of 14 nm observed when the interparticle distance P was varied from 200 to 300 nm. Nevertheless this result cannot be generalized as it may depend also on other parameters as the diameter and the height of cylinders. However the influence of the uncertainties on the height and the diameter of nanocylinders on the LSPR has still not been investigated. We focus on the systematic study of the position of LSPR as a function of the diameter D and height h of the gold nanocylinders. The influence of the thickness e of the adhesion layer and the roughness of surface are investigated.

http://dx.doi.org/10.5772/52906

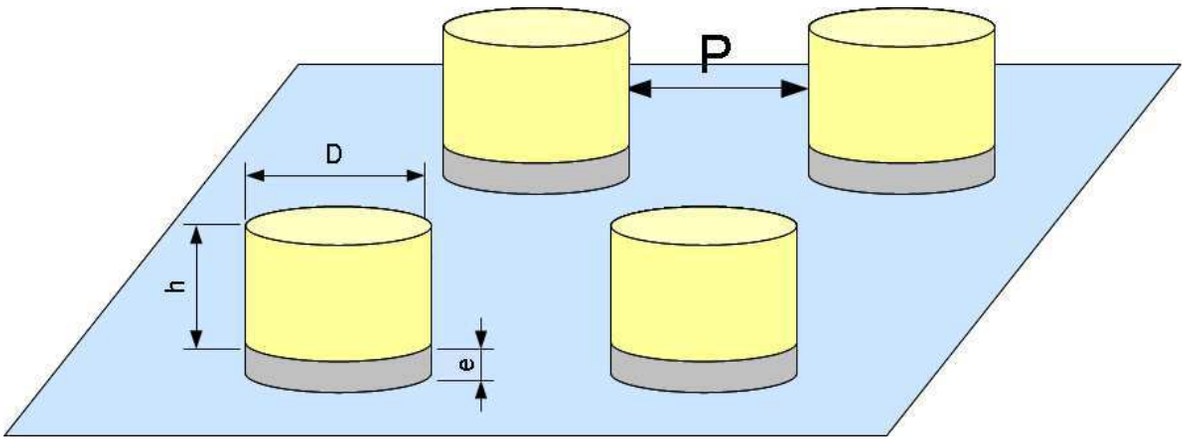

Figure 1. Biosensor: grating of gold cylinders with diameter D, height h and period $P + D$. The gold nanostructures are deposited on a CaF_2 substrate. A layer of Chromium of thickness e is used to improve adhesion of gold on CaF_2.

The nanostructures are deposited on a CaF_2 substrate through electron beam lithography (EBL) and lift-off techniques. To achieve EBL, a 30 kV Hitachi S-3500N scanning electron microscope (SEM) equipped with nanometer pattern generation system (NPGS, by J.C. Nabity) are used [8]. The SEM images [20, 21, 23, 37] reveal the experimental sources of uncertainties on the geometrical parameters in the process of fabrication:

- Height (h): the maximum uncertainty is $\delta_h = \pm 2$ nm. This value is due to both the roughness and the process of metal deposition. The SEM images and AFM (Atomic Force Microscopy) scans reveal a nanometric roughness with RMS (root of mean square) lower than one nanometer [20].
- Thickness (e): the maximum uncertainty is also $\delta_e \pm 2$ nm (same deposition technique), but may depend on the thickness of the intermediate layer.
- Diameter (D): the maximum uncertainty is $\delta_D = \pm 20$ nm. This value is relative to both the fabrication and the resolution of the SEM [41] and to a drift of diameter and shape on the whole grating. This last source of uncertainty is evaluated through statistics on the SEM images and is compatible with that found in literature [29].
- Cylinders separation (P): the maximum uncertainty is the same as that on D, $\delta_P = \pm 20$ nm, with some variations [19].

In the following, a numerical model (DDA) will be used to investigate the propagation of uncertainties on the position of the LSPR.

The illumination comes parallel to the cylinder axis and is linearly polarized. The detection of the LSPR is carried out in transmission, in the same direction (in the specular direction) and in far field. Spectroscopic studies are experimentally performed and the maximum of extinction over the incoming wavelengths λ_0 is supposed to reveal the LSPR position [5]. It is commonly admitted that the nanostructures scatter and absorb a part of the incoming light and that the detected intensity in transmission reveals the extinction of the illumination by the sample [9, 30].

2.2. The numerical model

2.2.1. The Discrete Dipole Approximation method

The measurement of the LSPR is made in far field and is modeled as the maximum of the extinction cross-section $C_{ext}(\lambda_0)$ (nm^2) with respect to the illumination wavelength λ_0 [9, 30]. The extinction cross section is the sum of the scattering and absorption cross sections. It corresponds to the rate of the total amount of incident electromagnetic energy abstracted from the incident beam due to interactions with particles.

The DDA is widely used for absorption, extinction and scattering calculations by nanoparticles [27] C_{ext} [15, 16, 37]. Its accuracy was checked by comparison to analytical solutions for spherical nanoparticles, ellipsoid [31], and infinite cylinder [16]. In what follows, a brief description of this method and of the numerical tool are given.

The method was firstly developed by [13, 14] and [38]. The main idea is to discretize the nanoparticle into a set of N elements or dipoles with polarizabilities α_j, located at $\mathbf{r}_j$. Each dipole has a polarization $\mathbf{P}_j = \alpha_j \mathbf{E}_j$, where $\mathbf{E}_j$ is the electric field at $\mathbf{r}_j$ induced by the incident wave and the sum of the dielectric fields induced by interaction with other dipoles. Consequently, a system of complex linear equations must be solved to find polarizations $\mathbf{P}_j$ and evaluate the extinction cross section following [15, Eq. (8) p. 1493]:

$$C_{ext} = Q_{ext}\pi\frac{D^2}{4} = \frac{4\pi k_0}{|\mathbf{E}_0|^2}\sum_{j=1}^{N}\left\{Im\left[\mathbf{P}_j.(\alpha_j^{-1})^*\mathbf{P}_j^*\right]\right\}, \tag{1}$$

with Q_{ext}, the extinction efficiency [9], $k_0 = 2\pi/\lambda_0$ the modulus of the wave vector and $\mathbf{E_0}$ the amplitude, of the illumination monochromatic plane wave. Im is the imaginary part of a complex number. C_{ext} is written under the assumption of linearly polarized incident light [15]. The method was extended to periodic structures by [34] and [10, 16].

2.2.2. Numerical parameters

The Fortran code DDSCAT 7.1, developed by Draine and Flatau, is used for calculating extinction of light by irregular particles based on the DDA [17]. DDSCAT offers the possibility of editing new shapes. Therefore, we edit the cylindrical shape to include the adhesion layer and the roughness. To simulate a realistic roughness, a uniform probability law is used to remove or to add a dipole from/to the surface, or to keep it unchanged. Therefore, the root of mean square roughness is RMS=$\sqrt{\frac{(-2)^2+0+2^2}{3}} \approx 1.6$ nm, that is close to the RMS that can be observed in MEB images of samples in abundant literature and websites.

The inter-dipole distance $d = 2$ nm is smaller than 2.6 nm that ensured the validity of the calculations in [19]. The target precision for the inversion of the matrix of coupling between dipoles is 10^{-3}. The magnitude of the electric field at distance r from any dipole decreases as a polynomial function of $1/r$. [16] introduced the factor $\exp\left[-(\gamma k_0 r)^4\right]$ to vanish the coupling between remote dipoles in a periodic lattice (with $k_0 = 2\pi/\lambda_0$ the modulus of the illumination wave vector) and therefore increase the speed and accuracy of computation. The cutoff parameter $\gamma = 0.1$ (which smoothly suppresses the influence of far dipoles in

periodic structures) is chosen to achieve both sufficient accuracy in the investigated size range of parameters, and a reasonable computational time over 12400 calculations. Indeed, for each structure with given h, D, e and roughness, the computation of spectrum in the range 550 nm to 850 nm of wavelength requires 31 evaluations of the model, if a precision of 10 nm is assumed sufficient for the LSPR spectral position.

The basis of the DDA being the discretization of materials, and therefore including the thick substrate in the model would be expensive. Consequently, the surrounding medium is modeled by an effective medium [24, 37] including the optical properties of the glass substrate [33] and air:

$$\epsilon_{eff} \approx (\epsilon_{air} + \epsilon_{CaF_2})/2 = 1.5267 \quad (2)$$

The relative permittivity of CaF_2 ($1.433^2 = 2.0535$) is considered as constant on the whole investigated domain of wavelengths ($\lambda_0 \in [550, 850]$ nm). The effective medium approximation may induce a blue-shift the LSPR [19], but the comparison with experimental data is able to validate directly this approximation and the choice of the optical properties for gold and chromium.

The optical properties of gold and chromium (the adhesion layer of thickness e) are the bulk ones [26, 36]. Chromium is more absorbing than gold and therefore the extinction spectrum is broadened and attenuated for Surface Plasmon resonance [7, 18, 35, 40] and nanostructured biosensors [35, 42].

To perform a parametric study, the optimum of dicretization of the parameter space (D, h, e λ_0) must be determined, by a first evaluation of the propagation of experimental uncertainties through the numerical model. The target is the position of the LSPR.

2.3. Propagation of experimental uncertainties on the position of the LSPR

The experimental uncertainties mentioned above (subsection 2.1) can help to define the step size of D, h, e and λ_0 in order to maintain the computational time of the parametric study in a reasonable range and to obtain significant results. For this, we compute the propagation of experimental uncertainties through the model to check their influence on the shift of the LSPR. Two diameters are considered for this evaluation with the above described model: $D = 100$ nm and $D = 200$ nm, near the boundaries of the investigated domain of the parametric study. The height of cylinders is the reference in experiments $h = 50$ nm [23]. A step of 10 nm is used for the computations of the spectrum $C_{ext}(\lambda_0)$. The cylinders are supposed to have smooth surfaces. The corresponding uncertainty on the position of LSPR ($\lambda_0(LSPR)$) is therefore ± 5 nm in the numerical calculations.

The combined uncertainty $u_B(\lambda_0(LSPR))$ on the LSPR shift can therefore be evaluated from the above uncertainties of type B [44], by considering *a priori* uniform law of probability within the above intervals and no correlation between these parameters. The following results are obtained:

- $D = 100$ nm, $h = 50$ nm, $P = 200$ nm [23].
  - For $P \in [180; 220]$ nm, the shift of the LSPR position is ± 5 nm.
  - For $D \in [80; 120]$ nm, the shift of the LSPR position is ± 20 nm.

- For $h \in [48;52]$ nm, the shift of the LSPR position is ± 30 nm.
- For $e \in [0;4]$ nm, the shift of the LSPR position is ± 10 nm.

$$u_B(\lambda_0(LSPR), D = 100nm) = \frac{1}{\sqrt{3}}\sqrt{5^2 + 20^2 + 30^2 + 10^2} = 21.8nm \quad (3)$$

- $D = 200$ nm, $h = 50$ nm, $P = 200$ nm [23].
  - For $P \in [180;220]$ nm, the shift of the LSPR position is ± 20 nm.
  - For $D \in [180;220]$ nm, the shift of the LSPR position is ± 30 nm.
  - For $h \in [48;52]$ nm, the shift of the LSPR position is ± 10 nm.
  - For $e \in [0;4]$ nm, the shift of the LSPR position is ± 10 nm.

$$u_B(\lambda_0(LSPR), D = 200nm) = \frac{1}{\sqrt{3}}\sqrt{20^2 + 30^2 + 10^2 + 10^2} = 22.4nm \quad (4)$$

In both cases, uncertainties may produce a shift greater than ± 20 nm within the investigated range of diameters. The results show that h and D are critical parameters for small diameter $D = 100$ nm. The influence of the uncertainty on the period seems to increase for larger diameters. The combined uncertainty is stable, even if the sensitivity to each source of uncertainty is not the same.

Consequently, the influence of the experimental uncertainties on the position of the LSPR can be observed considering a sampling step of 10 nm for λ_0. The corresponding uncertainty on the position of LSPR ($\lambda_0(LSPR)$) is therefore ± 5 nm in the numerical calculations. The evaluation of the experimental uncertainty (Eqs. 3 and 4) is used in the following.

The comparison of the model of smooth cylinders without adhesion layer and that with roughness and $e = 2$ nm, for some diameters reveals that the chromium layer and a RMS equal to 1.6 nm have also significant influence on the shift of the LSPR. For $D = 100$ nm, the shift is -40 nm, for $D =$130, 150 nm, the shift is $+10$ nm, and for $D = 180$, 200 nm, the shift is $+20$ nm. Therefore, the effect of these parameters on LSPR can be described with the above mentioned sampling for λ_0. Moreover, first trends emerge: the small cylinders exhibits a different behavior of the large ones.

The following subsections are devoted to the validation of the model by comparison with theoretical and experimental data.

2.4. Influence of the effective medium approximation

The comparison with other theoretical results may help to validate the proposed model of effective medium. In this first comparison, the reference is a theoretical study of the influence of a chromium adhesion layer with FDTD (Finite Difference Time Domain) method [42]. In that reference, no roughness was introduced, the surface of cylinders was smooth, $D = 100$ nm and $h = 50$ nm. The period of the grating was $D + P = 300$ nm with $P = 200$ nm (Figure 1). The relative permittivities were found in the same references [26, 36] and the nanostructures were deposited on a glass substrate. The intermediate layer had thickness 0, 1, 5, 30 nm. The location of the LSPR in the absence of Cr occurs at $\lambda_0 = 586$ nm with

http://dx.doi.org/10.5772/52906

FDTD and $\lambda_0 = 590$ nm with DDA. Therefore, we may conclude that the model of effective index is relevant, for the considered sample. [42] showed that if the Chromium adhesion layer is introduced, the spectrum curve is broadened and the maximum is blue-shifted, for $D = 100$ nm. For example, the LSPR was found at 541 nm for $e = 5$ nm and between 570 nm and 600 nm with the DDA (this interval is determined from eight DDA results with combinations of $D = 90$, $D = 110$ and $e = 4$, $e = 6$ nm). The blueshift of LSPR is less with DDA and effective index than with FDTD. Therefore, the comparison with experiments can help to decide on the ability of DDA to describe biosensors.

2.5. Validation of the DDA model with experimental data

The reference experimental data were published in [23, Fig. 2]. In that paper, the thickness of chromium $e = 3$ nm and the height of cylinders is 50 nm, with above mentioned experimental uncertainties. The computation of the position of the LSPR requires 31 computations of the extinction cross-section C_{ext} for $\lambda_0 \in [550; 850]$ nm. The smooth and rough samples are considered for the model. The relevance of the numerical results relies on using the experimental uncertainties to generate the corresponding intervals, for the position of the LSPR.

It is well known that increasing the diameter D or decreasing the height h of cylinders redshift the LSPR [37]. The above mentioned theoretical study [42] and our results show that including the adhesion layer blueshifts the LSPR for $D = 100$ nm. Therefore, the boundaries of the numerical results are chosen to find the minimum and the maximum of the LSPR position, according to the above mentioned sampling steps. For example, for experimental data with $e = 3$ nm, $D = 100$ nm, $h = 50$ nm, the interval of possible numerical position of LSPR is $[\lambda_0(LSPR, e = 4, D = 90, h = 52nm); \lambda_0(LSPR, e = 2, D = 110, h = 48nm)$. In Figs. 2 and 3, the computed LSPR is between the dashed and the solid lines for smooth (blue) and rough (red) structures.

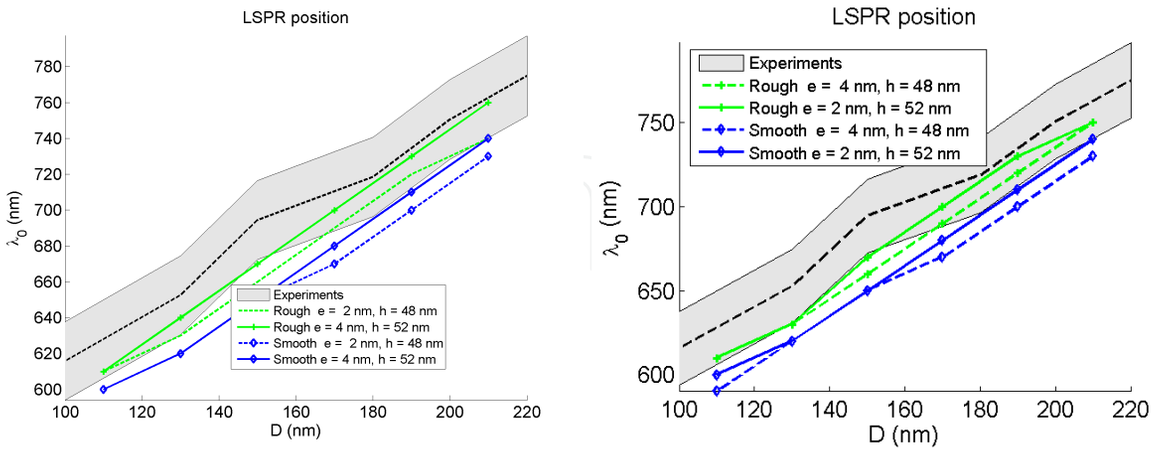

Figure 2. Experimental values (dashed black line) ($h = 50$, $e = 3$ nm) and uncertainties (gray, Eqs. 3 and 4), by courtesy of Nicolas Guillot and Marc Lamy de la Chapelle [23]. Extremal DDA results for smooth and rough structures, obtained by using experimental uncertainties on e and h.

Figure 2 shows a better agreement of simulation with rough surface than with smooth surface over the interval of diameters. The LSPR position for smooth cylinders is clearly blueshifted

and does not fall within the interval of experimental uncertainties. For $D = 100$ nm, $h = 50$ nm, $P = 200$ nm (Fig. 1), DDA gives $\lambda_0(LSPR) \in [603;628]$ which is closer to experiments [23] ($\lambda_0(LSPR) = 615\ nm$) than FDTD [42], where the LSPR was found between 541 nm ($e = 5$ nm) and 583 nm ($e = 1$ nm).

To evaluate the sensitivity of the results obtained by DDA with h, reference experimental data are extracted from [20] with $D = 100$ nm. Again, the agreement of experimental data with the numerical results for rough structures is better than for smooth ones. Both studies of LSPR position as a function of D and h show that the roughness produces a redshift, which is necessary to reproduce the experimental data, especially for the largest heights. This effect could also explain the blueshift obtained by [42] with smooth structures.

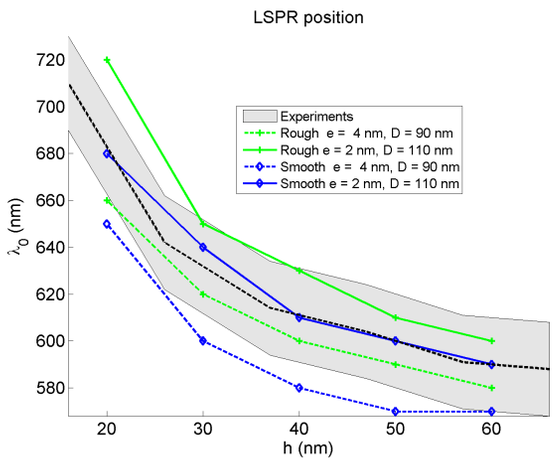

Figure 3. Experimental data from [20] (dashed line) ($D = 100$ nm, $e = 3$ nm) and uncertainty $u_B = \pm 20$ nm. Extremal DDA results for smooth and rough structures, obtained by using experimental uncertainties on e and D.

For each diameter D (Fig. 2) or height h (Fig. 3), the difference of LSPR between the dashed and solid lines can be considered as an evaluation of the sensitivity of the LSPR to the uncertainty on the thickness of chromium and on the size of structures. For all diameters the sensitivity is lower than 20 nm.

The comparisons of numerical results to experimental data show that the rough model with adhesion layer is more efficient to describe the experiments on a wide range of parameters. Moreover, the model of effective index for the external medium and the choice of the relative permittivities of gold and chromium seem to be adequate, as well as the exogenous parameters of the DDA (d, γ). Therefore, the proposed model can be used to provide full parametric study of the biosensor.

3. Parametric study

According to the experimental uncertainties, we have chosen an adapted sampling of each parameter of the model in subsection 2.3. The good agreement with the experimental data shown in the previous section confirms also the adequate choice of the exogenous parameters: the inter-dipole distance d, the cutoff parameter γ, the target precision of matrix inversion 10^{-3}, and the relative permittivities [26, 36]. The effective relative permittivity of the surrounding medium is given in Eq. 2.

http://dx.doi.org/10.5772/52906

Consequently, a systematic study of the LSPR position and its quality is produced for a class of nanostructured biosensors with cylindrical shapes. The quality of LSPR is given by the maximum over the spectral range of the extinction cross-section (C_{ext}): $\max_{\lambda_0} C_{ext}(D,h,e,RMS)$ or its relative dimming. The relative variation $\Delta_r C_{ext}$ of the quality of the plasmon corresponds to the attenuation of the LSPR:

$$\Delta_r C_{ext} = 100 \frac{\max_{\lambda_0}(C_{ext}(e)) - \max_{\lambda_0}(C_{ext}(0))}{\max_{\lambda_0}(C_{ext}(0))} \quad (5)$$

The influence of size parameters (D,h) for various adhesion layer (e) and roughnesses (RMS), on the tuning of the plasmon resonance is proposed.

The LSPR position and its quality are plotted in color levels, as functions of the height h and the diameter D. For the plots of the LSPR position ($\lambda_0(LSPR)$), the colors of rectangles are chosen to be close to the real colors [2] in the visible domain and vary from black to light pink for the near infrared. When the position of the LSPR is out off the considered range of wavelengths $[550;850]$ nm, a white rectangle is plotted.

The influence of the adhesion layer and of the roughness are successively investigated.

3.1. The adhesion layer

Figures 4 show the position of the LSPR and the maximum value of C_{ext} for an adhesion layer of thickness $e = 2,4$ and 6 nm. The maximum of C_{ext} is linked to the quality of the LSPR: the sensitivity of the biosensor is expected to be improved with the increase of the extinction cross-section. Increasing the thickness e produces a broadening of the spectrum which results in a decrease of $\max(C_{ext})$ and therefore of the quality of the LSPR as defined above.

For the three thicknesses of chromium the position of the LSPR is about the same but the quality of LSPR is deteriorated if e growth. The position of the LSPR is redshifted if the diameter D of cylinders is increased. This conclusion was underlined in [23]: "Indeed, as it is well known, the position of the LSPR is redshifted for higher diameter". The height h influences also the position of the LSPR: for a given diameter, if h increases, the LSPR is blueshifted. These conclusions are also consistent with previous studies of cylindrical nanorods [37].

The LSPR shift (nm) and $\Delta_r C_{ext}$ are displayed in Fig. 5. Even if the LSPR shift may be considered as negligible with regards to the influence of the uncertainties of fabrication, the relative attenuation of the LSPR can reach more than 45% for the smallest D and h. Therefore, the adhesion layer cannot be neglected if the efficiency of the biosensor is targeted. The chromium (and all adhesion layers) being more absorbing, it deteriorates the efficiency of the biosensor and therefore, its thickness should be reduced as much as possible.

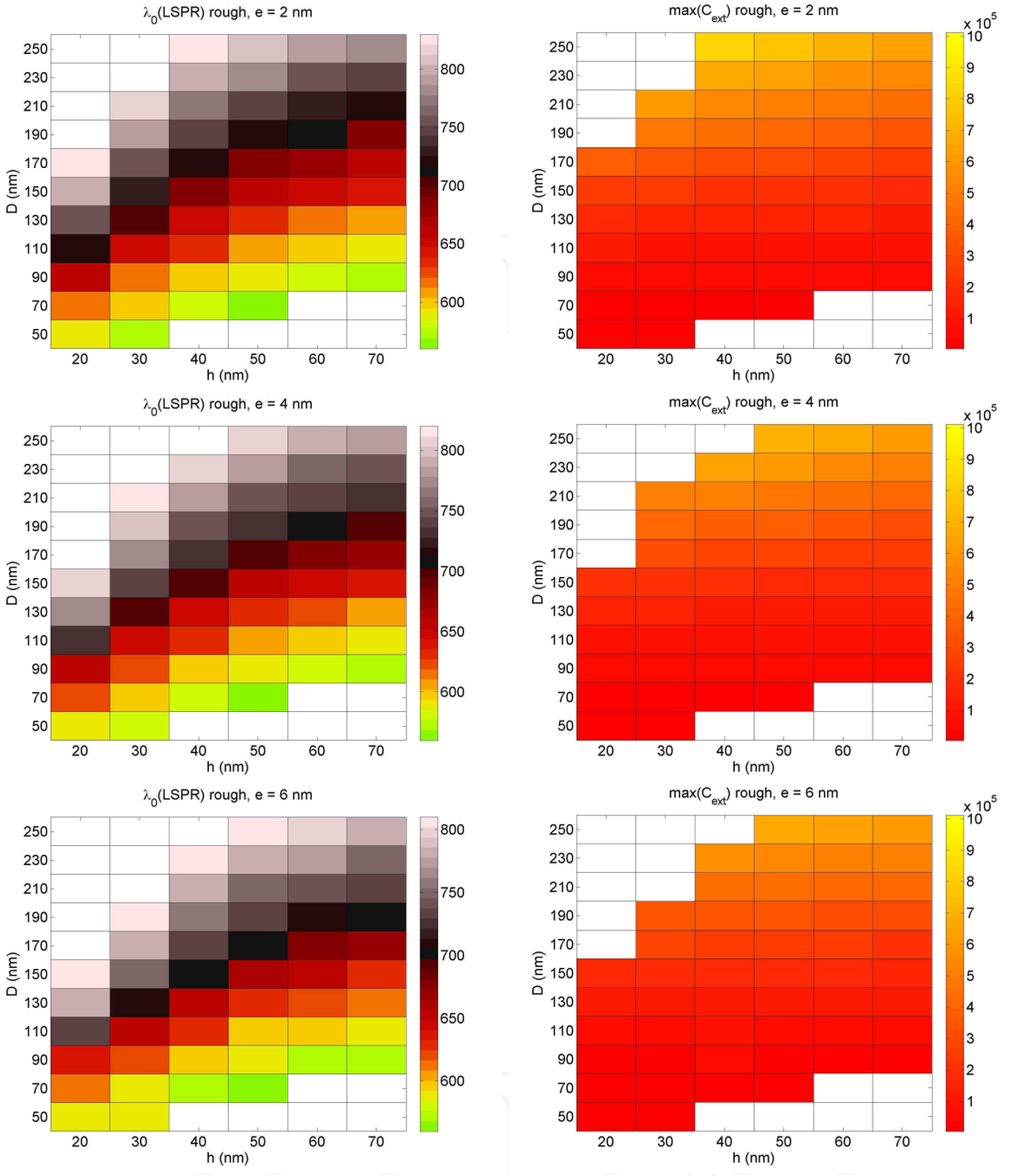

Figure 4. Numerical parametric study of the cylinder based biosensor: position of the LSPR ($\lambda_0(LSPR)$) and its quality illustrated by the maximum of C_{ext} (nm^2) as functions of the diameters D and heights h of the nanocylinders, for different thicknesses of the adhesion layer $e = 2$, $e = 4$ and $e = 6$ nm.

3.2. The roughness

A similar set of simulations could reveal the influence of the roughness (Fig. 6).

The roughness has less influence on the quality of plasmon than e. This influence decreases when D and h increases. The relative influence of the roughness decreases if the thickness e of the adhesion layer increases and becomes lower than 20% if $e > 4$ nm. In the case of pure gold ($e = 0$ nm), the roughness induces a decrease (less than 20%) of $\max(C_{ext})$ for small

http://dx.doi.org/10.5772/52906

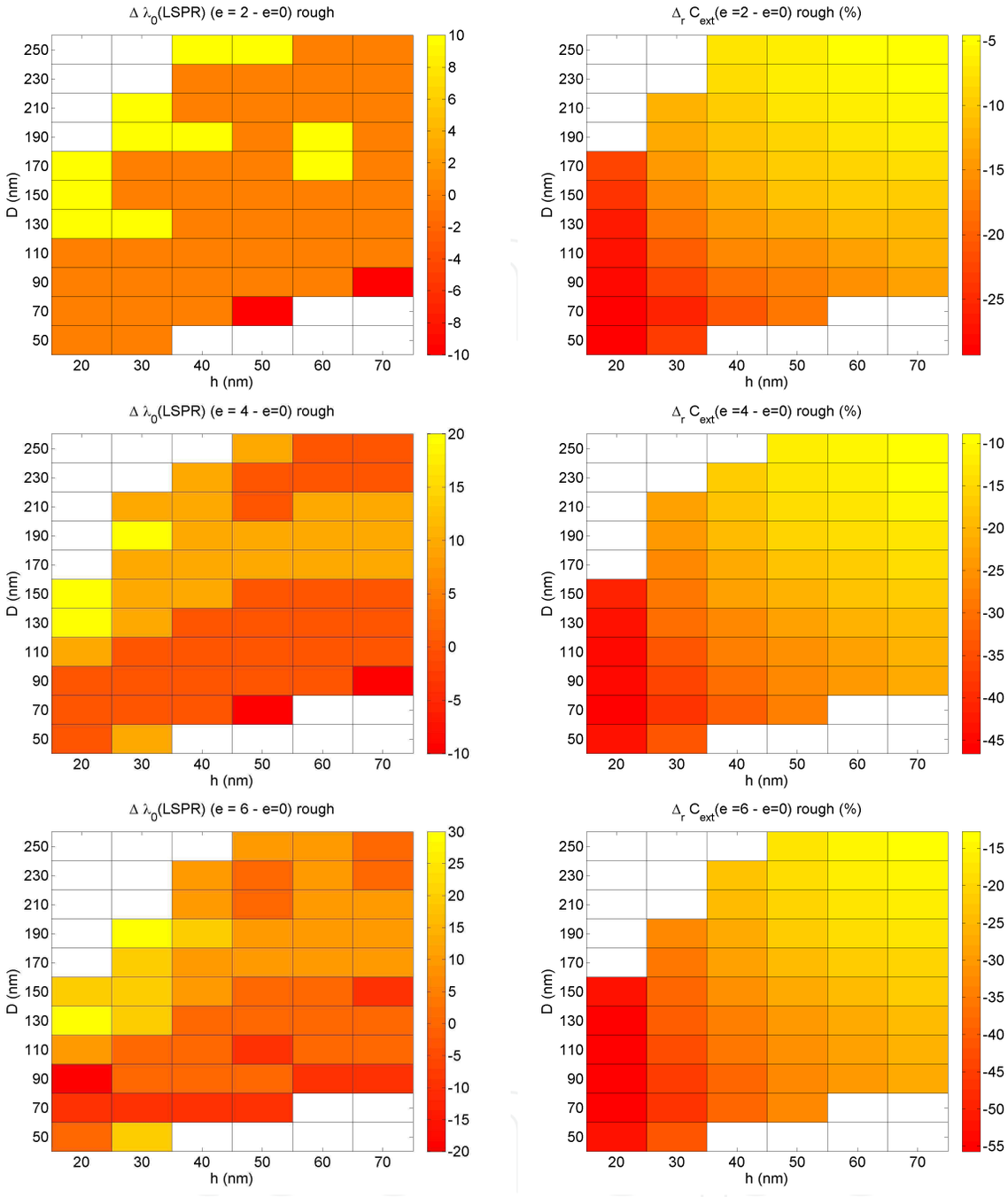

Figure 5. Numerical parametric study of the cylinder based biosensor: shift of the position of the LSPR $\Delta\lambda_0(LSPR)$ (nm) and its quality $\Delta_r C_{ext}$ (Eq. 5) as functions of the diameters D and heights h of the nanocylinders, for thicknesses of the adhesion layer $e = 2$, $e = 4$ and $e = 6$ nm, with reference to $e = 0$.

diameters and small height, and an increase (also less than 20%) for larger values of D and h. The redshift of the LSPR can reach 40 nm for small heights and average diameters. This effect can be explained by the increase of the ratio of the area of rough surface of the cylinder to its height. The effect of the roughness is reduced when the volume of cylinder increases. The shift of the LSPR becomes negligible for the highest and largest cylinders. The LSPR is redshifted in almost all the cases, when roughness is introduced. The redshift is smaller than 40 nm for all the investigated adhesion layers.

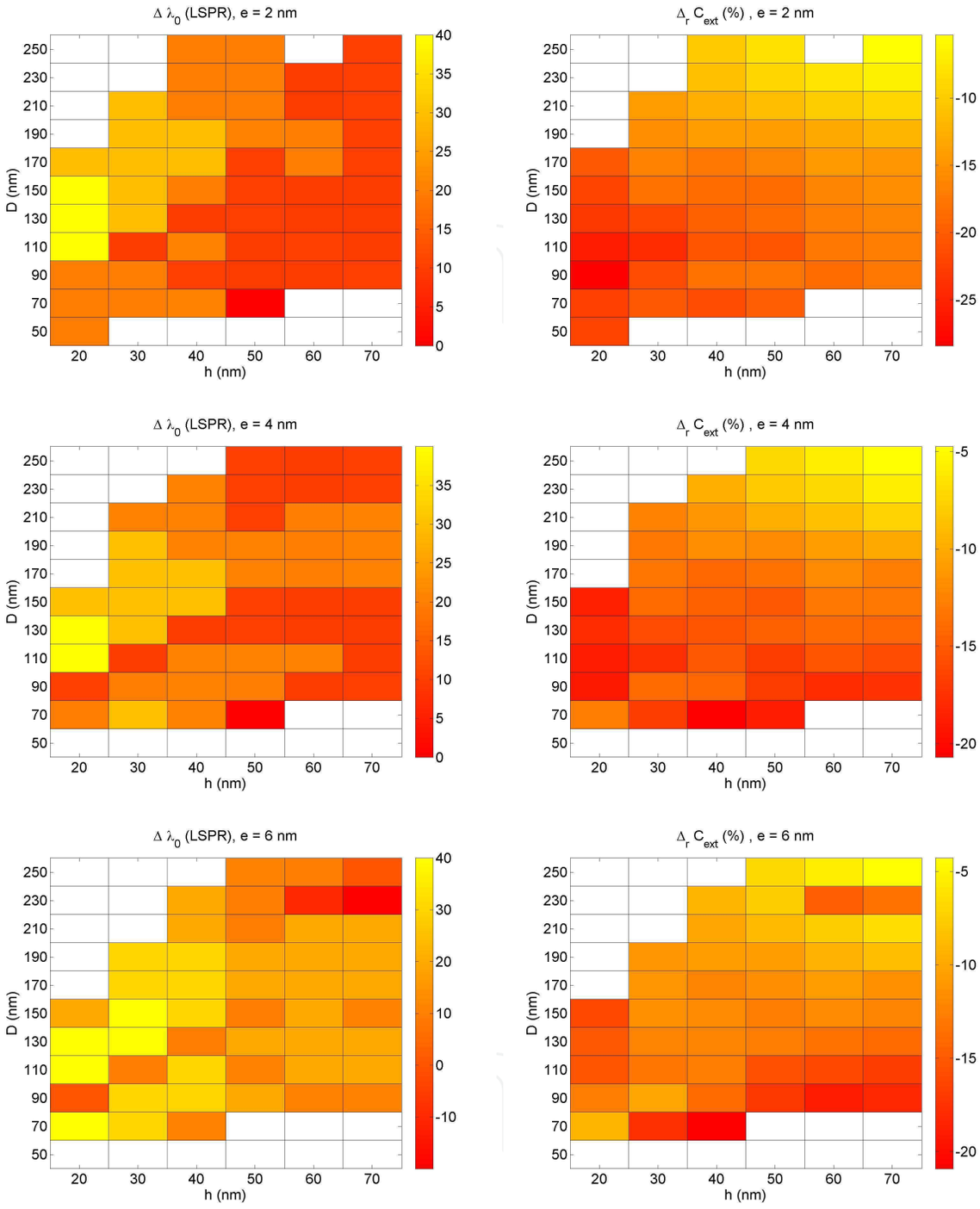

Figure 6. Numerical parametric study of the cylinder based biosensor: shift of the position of the LSPR $\Delta\lambda_0(LSPR)$ (nm) and its relative quality $\Delta_r C_{ext}$ (Eq. 5) as functions of the diameters D and heights h of the nanocylinders, for thicknesses of the adhesion layer $e = 2$, $e = 4$ and $e = 6$ nm, with reference to the smooth structure.

The diameter D and the height h seem to be linearly connected for a given LSPR position as it can be observed in Fig. 4. This linear behavior can lead to heuristic law which can be used to study the propagation of uncertainties.

http://dx.doi.org/10.5772/52906

4. Heuristic law for LSPR

4.1. The LSPR $\lambda_0(LSPR)(D,h)$

For both thicknesses of the chromium adhesion layer $e = 2$ and $e = 6$ nm, the position of LSPR is about the same when both D and h are varied respectively by 20 nm and 10 nm, with $P = 200$ nm, and a roughness of RMS= 1.6 nm. The resulting behavior law can be deduced from the parametric study: a steady position of the LSPR is observed, if the following law between D (nm) and h (nm) is satisfied:

$$D(P = 200, e = 2-6) = ah + b \approx (0.0084\lambda_0(LSPR) - 3.86)h + (0.319\lambda_0(LSPR) - 160) \quad (6)$$

This law is deduced from the least square fit of the results of the parametric study, simply by computing the slope and the intercept of D as a function of h for each LSPR position, and then by finding the linear dependence of a and b on the LSPR position $\lambda_0(LSPR)$. A similar approach was used to characterize the near-field optical microscopes and the evanescent near-field around nanostructures [1, 4]. The method uses a robust fit of the results of the parametric study. The algorithm uses iteratively reweighted least squares with the bisquare weighting function (Matlab).

Figure 7 shows the plots of Eq. 6, superimposed on figures 4. The linear behavior of D as a function of h is dependent on the LSPR position. Equation 6 helps to determine the geometrical parameters (D and h) of the biosensor to adjust the LSPR to a given wavelength.

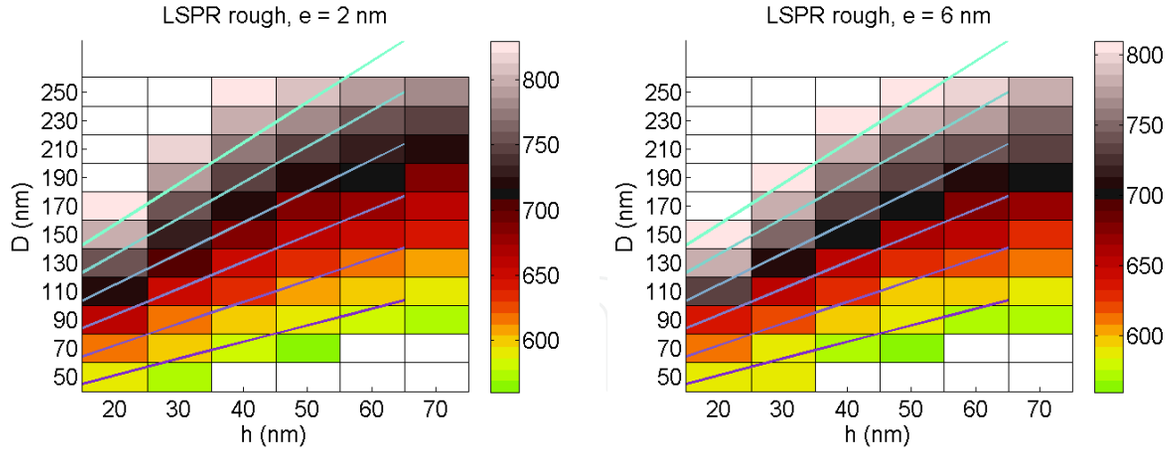

Figure 7. Plots of D as a function of h for $\lambda_0(LSPR) \in \{600; 640; 680; 720; 760; 800\}$ from Eq. 6.

Similarly, the position of the LSPR (nm) can be deduced from Eq. 6 as a function of D (nm) and h (nm):

$$\lambda_0(LSPR) \approx \frac{160 + D + 3.86h}{0.319 + 0.0084h} \quad (7)$$

A comparison of the simple model (Eq. 7) and experimental data in [21] shows a good agreement. Equation 7 seems to be a good approximation of the variation of the LSPR as a function of the geometrical parameters D and h, for a grating of rough gold cylinders with adhesion layer ($e = 2$ nm) and $P = 200$ nm (Fig. 1). The specific case of homothetic cylinders with $h = D$, removes a degree of freedom and leads to a simpler formula:

$$\lambda_0(LSPR, h = D) = \frac{160 + 4.86D}{0.319 + 0.0084D} \tag{8}$$

This formula is strictly valid in the interval $h = D$ ranging from 50 to 70 nm, by cons it should still be checked for greater heights.

Asymptotic form of $\lambda_0(LSPR)$ could be of interest especially for specific aspect ratio of the cylinder. For example, for nanodiscs ($h << D$), the position of the LSPR can be deduced from the series of Eq. 7.

$$\lambda_0(LSPR, h << D) = (501 + 3.1D) - (0.0825D + 1.1)h + o[(h/D)^2], \tag{9}$$

where $o[(h/D)^2]$ represents omitted terms of order higher than 2 in the series.

This equation confirms that the correction induced by the height assuming a small aspect ratio h/D is a blueshift of the LSPR, whatever are the diameters D. These formula can be used to select the best parameters for a given LSPR position. Another interest of these simple laws is the fact that propagation of uncertainties of the fabrication process can be evaluated directly, and therefore, the sensitivity analysis of LSPR position on the geometrical parameters h and D can be deduced, at least within the investigated domain of geometrical parameters and wavelengths. This sensitivity analysis is conducted in what follows.

4.2. Sensitivity of LSPR to uncertainties on size parameters

The propagation of uncertainties and the sensitivity analysis of a process or a physical phenomenon helps to improve the fabrication process of any device, by exhibiting the parameters that should be controlled first. Indeed the identification of critical parameters which uncertainty should be reduced is relevant, for a challenging improvement of technology.

First, the propagation of experimental uncertainties of fabrication can be deduced from the derivative of Eq. 7. The uncertainty on $\lambda_0(LSPR)$ is deduced form the uncertainties on D ($u(D)$) and h ($u(h)$) [44, 5.1.2]:

$$u(\lambda_0(LSPR)) = \sqrt{\left(\frac{\partial \lambda_0(LSPR)}{\partial D}\right)^2 u^2(D) + \left(\frac{\partial \lambda_0(LSPR)}{\partial h}\right)^2 u^2(h)}, \tag{10}$$

where the partial derivatives are called sensitivity coefficients. Using Eq. 7 gives:

http://dx.doi.org/10.5772/52906

$$u(\lambda_0(LSPR)) = \sqrt{\left(\underbrace{\frac{1}{0.319+0.0084h}}_{S_D}\right)^2 u^2(D) + \left(\underbrace{\frac{0.11266+0.0084D}{(0.319+0.0084h)^2}}_{S_h}\right)^2 u^2(h)} \qquad (11)$$

Knowing the experimental uncertainties on h and D, the uncertainty on the LSPR can be deduced. The sensitivity coefficients S_h and S_D can be used to evaluate the effect of the experimental dispersion of values of D and h around a mean value. S_D is almost independent of h and equal to 3. Regarding S_h and within the same approximation $S_h \approx 1.107 + 0.082D$. Therefore, in the investigated domain of D, $S_h \in [5.2; 21.6]$. The uncertainty on h must be 7 times smaller than that on D to balance the contributions of each uncertainty to the overall uncertainty. This condition is becoming increasingly critical as the diameter D of cylinders is increased. Fortunately, the control on the thickness of gold deposition (height of cylinders) is about ± 2 nm and that of diameters is about ± 20 nm. In this case, the uncertainty on the LSPR position remains lower than 30 nm for all diameters if $h > 40$ nm (Fig.8).

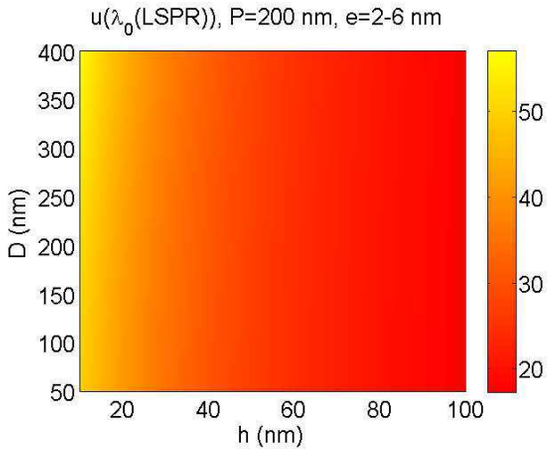

Figure 8. Uncertainty on the position of the LSPR computed from the heuristic law (Eq. 11) deduced from the least square fit of the parametric study results. The parameters of the model are $P = 200$ nm with roughness ($rms = 1.6$ nm) and chromium adhesion layer ($e = 2 - 6$ nm).

Figure 9 gathers the experimental results retrieved from [23] with experimental uncertainties (gray domain and) the heuristic law deduced from Eq. 7 with uncertainties (Eq. 10). The good agreement between experimental results and the heuristic model with associated uncertainties can be observed. The heuristic model fits well the experimental data and the uncertainties deduced from Eq. 11 are coherent with the experimental ones.

In this section, we have obtained an heuristic law to describe the link between the position of the LSPR and the size parameters D and h of the cylinders. This law seems to be valid for an adhesion layer of chromium of thickness $e = 2 - 6$ nm. Moreover, the simplicity of this law helps to determine a first approximation of the size of the cylinder, as well as the effect of the propagation of experimental uncertainties on the position of the LSPR.

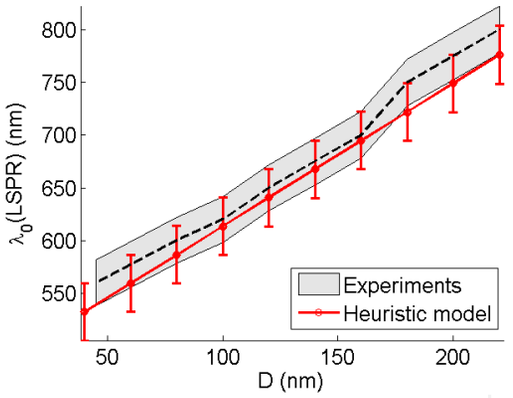

Figure 9. Experimental data retrieved from [23, Fig. 2] ($h = 50$ nm, $e = 3$ nm, $P = 200$ nm) (black) with uncertainties (gray). Heuristic model deduced from the numerical parametric study of gold nanocylinder grating (red curve) with $P = 200$ nm, $h = 50$ nm, RMS 1.6 nm and chromium adhesion layer ($e = 4$ nm).

5. Conclusion

A model based on the Discrete Dipole Approximation (DDA) is used for a parametric study of the biosensors made of a grating of nanocylinders. The Localized Surface Plasmon Resonance (LSPR) is modeled by the position of the maximum over the spectrum of the extinction cross-section. The investigated parameters are the height h, the diameter D, the thickness e of the chromium adhesion layer, and the roughness of the nanocylinders. Thin adhesion layers slightly modify the position of the LSPR but degrade significantly its quality: the sensitivity of the biosensor can be highly decreased. Roughness induces a redshift of the LSPR but less alters the quality of the resonance than the adhesion layer. The relative influence of h and D is more complex. Actually, if D increases, a redshift is always observed. The same effect occurs if h decreases. Consequently the fine tuning of the LSPR can be achieved by varying D or h, assuming a fixed distance between cylinders (P). This property helps to deduce heuristic laws for the LSPR position and the propagation of uncertainties. The basic law, deduced from a least square fit, gives simply an approximation of the position of the LSPR as a function of D and h. The agreement with experimental results [21, 23] is satisfactory, falling within the experimental uncertainties of fabrication. Therefore the heuristic law of behavior of the LSPR position can be used with confidence (for $P = 200$ nm). Varying the period $P + D$ of the grating of nanocylinders could be of interest. The characterization of the LSPR being clarified, the influence of the functionalization layer will be the object of future studies.

Acknowledgment

This work was supported by the “Conseil Régional de Champagne Ardennes”, the “Conseil Général de l’Aube” and the *Nanoantenna* European Project (FP7 Health-F5-2009-241818).

Author details

Sameh Kessentini and Dominique Barchiesi

Automatic Mesh Generation and Advanced Methods (GAMMA3 - UTT/INRIA) - Charles Delaunay Institute - University of Technology of Troyes - Troyes, France

http://dx.doi.org/10.5772/52906

References

[1] Barchiesi, D. [1998]. Pseudo modulation transfer function in reflection scanning near-field optical microscopy, *Optics Communications* 154: 167–172.

[2] Barchiesi, D. [2008]. Simulations d'expériences faisant intervenir la couleur : dispersion par un prisme et réflectance, *Bulletin de l'Union des Professeurs de Physique Chimie* 909 (102)(1): 1369–1382.

[3] Barchiesi, D. [2011]. *New Perspectives in biosensors technology and applications*, INTECH Open Access, Rijeka, Croatia, chapter 5, pp. 105–126.
URL: *http://cdn.intechweb.org/pdfs/14870.pdf*

[4] Barchiesi, D., Bergossi, O., Spajer, M. & Pieralli, C. [1997]. Image resolution in reflection scanning near-field optical microscopy (R-SNOM) using shear-force (ShF) feedback: Characterization using spline and Fourier spectrum, *Appl. Opt.* 36(10): 2171–2177.

[5] Barchiesi, D., Kremer, E., Mai, V. & Grosges, T. [2008]. A Poincaré's approach for plasmonics: The plasmon localization, *J. Microscopy* 229: 525–532.

[6] Barchiesi, D., Lidgi-Guigui, N. & Lamy de la Chapelle, M. [2012]. Functionalization layer influence on the sensitivity of surface plasmon resonance (SPR) biosensor, *Optics Communications* 285(6): 1619–1623.

[7] Barchiesi, D., Macías, D., Belmar-Letellier, L., Van Labeke, D., Lamy de la Chapelle, M., Toury, T., Kremer, E., Moreau, L. & Grosges, T. [2008]. Plasmonics: Influence of the intermediate (or stick) layer on the efficiency of sensors, *Appl. Phys. B* 93: 177–181.

[8] Billot, L., M. Lamy de la Chapelle, Grimault, A. S., Vial, A., Barchiesi, D., Bijeon, J.-L., , Adam, P.-M. & Royer, P. [2006]. Surface enhanced Raman scattering on gold nanowire arrays: Evidence of strong multipolar surface plasmon resonance enhancement, *Chem. Phys. Lett.* 422(4-6): 303–307.

[9] Bohren, C. F. & Huffman, D. R. [1998]. *Absorption and Scattering of Light by Small Particles*, John Wiley & Sons, Inc., New York.

[10] Chaumet, P. C., Rahmani, A. & Bryant, G. W. [2003]. Generalization of the coupled dipole method to periodic structures, *Phys. Rev. B* 67(16): 165404(1–5).

[11] Dasgupta, A. & Kumar, G. V. P. [2012]. Palladium bridged gold nanocylinder dimer: plasmonic properties and hydrogen sensitivity, *Appl. Opt.* 51(11): 1688–1693.

[12] Davy, S., Barchiesi, D., Spajer, M. & Courjon, D. [1999]. Spectroscopic study of resonant dielectric structures in near–field, *European Physical Journal (Applied Physics)* 5: 277–281.

[13] Devoe, H. [1964]. Optical properties of molecular aggregates. I. classical model of electronic absorption and refraction, *J. Chem. Phys.* 41: 393–400.

[14] Devoe, H. [1965]. Optical properties of molecular aggregates. II. classical theory of the refraction, absorption, and optical activity of solutions and crystals, *J. Chem. Phys.* 43: 3199–3208.

[15] Draine, B. T. & Flatau, P. J. [1994]. Discrete-dipole approximation for scattering calculations, *J. Opt. Soc. Am. A* 11: 1491–1499.

[16] Draine, B. T. & Flatau, P. J. [2008]. Discrete-dipole approximation for periodic targets: Theory and tests, *J. Opt. Soc. Am. A* 25: 2693–2703.

[17] Draine, B. T. & Flatau, P. J. [2010]. User guide to the discrete dipole approximation code DDSCAT 7.1, http://arXiv.org/abs/1002.1505v1.

[18] Ekgasit, S., Thammacharoen, C., Yu, F. & Knoll, W. [2005]. Influence of the metal film thickness on the sensitivity of surface plasmon resonance biosensors, *Appl. Spectroscopy* 59: 661–667.

[19] Félidj, N., Aubard, J., Lévi, G., Krenn, J. R., Salerno, M., Schider, G., Lamprecht, B., Leitner, A. & Aussenegg, F. R. [2002]. Controlling the optical response of regular arrays of gold particles for surface-enhanced Raman scattering, *Phys. Rev. B* 65: 075419–075427.

[20] Grand, J. [2004]. *Plasmons de surface de nanoparticules : spectroscopie d'extinction en champs proche et lointain, diffusion Raman exaltée*, PhD thesis, Université de technologie de Troyes.

[21] Grand, J., Lamy de la Chapelle, M., Bijeon, J.-L., Adam, P.-M., Vial, A. & Royer, P. [2005]. Role of localized surface plasmons in surface-enhanced raman scattering of shape-controlled metallic particles in regular arrays, *Phys. Rev. B* 72(3): 033407.

[22] Grimault, A.-S., Vial, A. & Lamy de la Chapelle, M. [2006]. Modeling of regular gold nanostructures arrays for SERS applications using a 3D FDTD method, *Appl. Phys. B* 84(1-2): 111–115.

[23] Guillot, N., , Shen, H., Frémaux, B., Péron, O., Rinnert, E., Toury, T. & Lamy de la Chapelle, M. [2010.]. Surface enhanced Raman scattering optimization of gold nanocylinder arrays: Influence of the localized surface plasmon resonance and excitation wavelength, *Appl. Phys. Lett.* 97(2): 023113–023116,.

[24] Haija, A. J., Freeman, W. L. & Roarty, T. [2006]. Effective characteristic matrix of ultrathin multilayer structures, *Optica Applicata* 36: 39–50.

[25] Huang, X., Neretina, S. & El-Sayed, M. A. [2009]. Gold nanorods: From synthesis and properties to biological and biomedical applications, *Advanced Materials* 21: 4880–4910.

[26] Johnson, P. & Christy, R. W. [1972]. Optical constants of the noble metals, *Phys. Rev. B* 6: 4370.

[27] Kessentini, S. & Barchiesi, D. [2012]. Quantitative comparison of optimized nanorods, nanoshells and hollow nanospheres for photothermal therapy, *Biomed. Opt. Express* 3(3): 590–604.

[28] Lamprecht, B., Schider, G., Lechner, R. T., Diltbacher, H., Krenn, J. R., Leitner, A. & Aussenegg, F. R. [2000]. Metal nanoparticles gratings: influence of dipolar interaction on the plasmon resonance, *Phys. Rev. Lett.* 84: 4721–4723.

[29] Laurent, G., Félidj, N., Aubard, J., Lévi, G., Krenn, J. R., Hohenau, A., Schider, G., Leitner, A. & Aussenegg, F. R. [2005]. Evidence of multipolar excitations in surface enhanced Raman scattering, *Phys. Rev. B* 65: 045430–1–045430–5.

[30] Le Ru, E. C. & Etchegoin, P. G. [2009]. *Principles of Surface-Enhanced Raman Spectroscopy and related plasmonic effects*, 1 edn, Elsevier, Amsterdam.

[31] Lee, K. S. & El-Sayed, M. A. [2005]. Dependence of the enhanced optical scattering efficiency relative to that of absorption of gold metal nanorods on aspect ratio, size, end-cap shape, and medium refractive, *J. Phys. Chem. B* 109: 20331–20338.

[32] Maier, S. A. [2007]. *Plasmonics. Fundamentals and Applications*, Springer, New York, USA.

[33] Malitson, I. H. [1963]. A redetermination of some optical properties of calcium fluoride, *Applied Optics* 2: 1103–1107.

[34] Markel, V. A. [1992]. Scattering of light from two interacting spherical particles, *J. Mod. Opt.* 39(4): 853–861.

[35] Neff, H., Zong, W., Lima, A., Borre, M. & Holzhüter, G. [2006]. Optical properties and instrumental performance of thin gold films near the surface plasmon resonance, *Thin Solid Films* 496: 688–697.

[36] Palik, E. D. [1985]. *Handbook of Optical Constants*, Academic Press Inc., San Diego USA.

[37] Pelton, M., Aizpurua, J. & Bryant, G. W. [2008]. Metal-nanoparticles plasmonics, *Laser & Photon. Rev.* 2(3): 136–159.

[38] Purcell, E. & Pennypacker, C. R. [1973]. Scattering and absorption of light by nonspherical dielectric grains, *Astrophysical Journal* 186: 705–714.

[39] Raether, H. [1988]. *Surface Plasmons on Smooth and Rough Surfaces and on Gratings*, Springer-Verlag, Berlin.

[40] Sexton, B. A., Feltis, B. N. & Davis, T. J. [2008]. Effect of surface roughness on the extinction-based localized surface plasmon resonance biosensor, *Sensors and Actuators A Physical* 141: 471Ű475.

[41] Sharma, D., Sharma, R., Dua, S. & Ojha, V. N. [2012]. Pitch measurements of 1D/2D gratings using optical profiler and comparison with SEM /AFM, *AdMet 2012*, Metrology Society of India, ARAI, Pune, India, pp. NM 003, 1–4.

[42] Vial, A. & Laroche, T. [2007]. Description of dispersion properties of metals by means of the critical points model and application to the study of resonant structures using the FDTD method, *J. Phys. D: Appl. Phys.* 40: 7152–7158.

[43] Vidotti, M., Carvalhal, R. F., Mendes, R. K., Ferreira, D. C. M. & Kubota, L. T. [2011]. Biosensors based on gold nanostructures, *J. Braz. Chem. Soc.* 22(1): 3–20.

[44] Working Group 1 [2008]. *Evaluation of measurement data - Guide to the expression of uncertainty in measurement*, 1 edn, Joint Committee for Guides in Metrology, Paris. Corrected version 2010.

[45] Yan, H.-H., Xiao, Y.-Y., Xie, S.-X. & Li, H.-J. [2012]. Tunable plasmon resonance of a touching gold cylinder arrays, *J. At. Mol. Sci.* 3(3): 252–261.

[46] Yanik, A. A., Huang, M., Artar, A., Chang, T.-Y. & Altug, H. [2010]. On-chip nanoplasmonic biosensors with actively controlled nanofluidic surface delivery, *in* M. I. Stockman (ed.), *Plasmonics: Metallic Nanostructures and Their Optical Properties VIII*, Vol. 7757, SPIE, San Diego, California, USA, pp. 775735–1–6.